Process Damping Milling Model Database

Christopher T. Tyler and Tony L. Schmitz
Mechanical Engineering and Engineering Sciences
University of North Carolina at Charlotte
Charlotte, NC

ABSTRACT
The paper describes an analytical milling stability model that includes process damping and presents a database of the process modeling coefficients for selected hard-to-machine materials: 1018 steel, 6Al-4V titanium, and 304 stainless steel. The velocity-dependent process damping force applied in the analysis relies on a single coefficient that is obtained experimentally. The database includes coefficients for the process damping model, specific cutting force, and Taylor tool life model. Coefficients are provided for two relief angles and at both low and moderate wear states. Additionally, a wavelength parameter is presented that enables the traditional analytical stability model to incorporate the process damping stability increase observed at low cutting speeds. It is proposed that this database will provide a valuable starting point for hard-to-machine material milling applications.

KEYWORDS
Milling, Modeling, Process damping, Stability, Tool wear

INTRODUCTION

Milling stability behavior can be predicted based on the selected spindle speed and axial depth of cut (for a selected radial depth of cut) using the well-known analytical stability lobe diagram [1-4]. However, the allowable increase in axial depth made possible by the selection of a tooth passing frequency near an integer fraction of the system's dominant natural frequency is reduced at low spindle speeds where the stability lobes are closely spaced. At these low speeds, the process damping effect can serve to increase the chatter-free axial depth of cut and enable higher material removal rates than the traditional stability analysis predicts. This increased stability for low spindle speeds is important for hard-to-machine materials that cannot take advantage of the higher speed stability zones due to prohibitive tool wear at high cutting speeds.

Early investigations of process damping in turning and milling operations were carried out by Wallace and Andrew [5], Sisson and Kegg [6], Peters *et al.* [7], and Tlusty [8]. More recently, researchers have described:

- a plowing force model based on the interference between the tool and workpiece [9]
- the application of this plowing force model to milling operations [10-13]
- a mechanistic description of the contributions of shearing and plowing forces to process damping [14]
- a first-order Fourier transform representation of the interference between the tool and workpiece [15-16]
- numerical simulation of the nonlinear process damping stability model [17-18]
- an experimental investigation of the nonlinear process damping stability model [19]
- experimental identification of the process damping model [20-21]
- an analytical stability model [22-23] that includes process damping based on the Tlusty *et al.* stability analysis [3].

These studies described process damping as energy dissipation due to interference between the cutting tool clearance face and machined surface during relative vibrations between the tool and workpiece. It was shown that, given fixed system dynamics, the influence of process damping increases at low spindle speeds because the number of undulations on the machined surface between revolutions/teeth increases, which also increases the slope of the wavy surface. This, in turn, leads to increased interference and additional energy dissipation.

In this paper, a database of the process modeling coefficients for selected hard-to-machine materials (1018 steel, 6Al-4V titanium, and 304 stainless steel) is presented. The database includes coefficients for the process damping model, specific cutting force, and Taylor tool life model. The analytical milling stability model includes a velocity-dependent process damping force that

uses a single empirical coefficient. The coefficients are provided for two relief angles at both low and moderate wear states of the cutting edge. Additionally, a wavelength parameter is presented that enables the traditional analytical stability model to be augmented to incorporate the process damping stability increase observed at low cutting speeds.

The paper is organized as follows. In the first section, process damping is described and the process damping force model is defined. Next, the stability algorithm is reviewed [22-23]. After, the experimental setup is detailed and then the database is presented. This is followed by the conclusions.

PROCESS DAMPING DESCRIPTION

In descriptions of regenerative chatter in machining, the variable component of the instantaneous cutting force may be written as:

$$F = K_s b (Y_0 - Y), \tag{1}$$

where K_s is the specific cutting force (which depends on the tool-workpiece combination and, to a lesser extent, the cutting parameters), b is the chip width, Y_0 is the vibration amplitude in the surface normal direction, y, from the previous cutting pass, and Y is the current vibration amplitude. See Fig. 1. The underlying assumption in Eq. 1 is that there is no phase shift between the variable force and chip thickness; this is indicated by the real values of K_s and b. However, for low cutting speeds, V, it has been shown that a phase shift can occur. This behavior is captured by the phenomenon referred to as process damping. Practically speaking, the effect of process damping is to enable significantly higher chip widths at low cutting speeds than linear stability analyses predict.

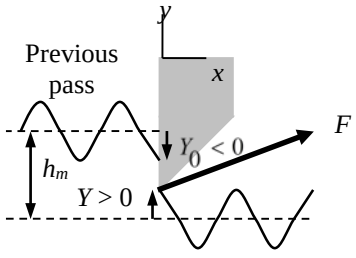

Figure 1. The variable component of the cutting force, F, depends on the instantaneous chip thickness. The chip width is measured into the page; the mean chip thickness, h_m, is also identified.

To describe the physical mechanism for process damping, consider a tool moving on a sine wave while shearing away the chip [24]; see Fig. 2. Four locations are identified: 1) the clearance angle, γ, between the flank face of the tool and the work surface tangent is equal to the nominal relief angle for the tool; 2) γ is significantly decreased and can become negative (which leads to interference between the tool's relief face and surface); 3) γ is again equal to the nominal relief angle; and 4) γ is significantly larger than the nominal value.

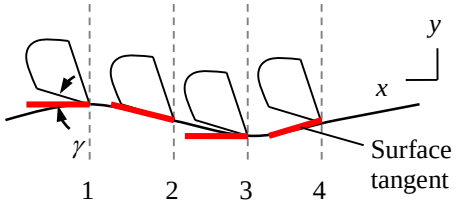

Figure 2. Physical description of process damping. The clearance angle varies with the instantaneous surface tangent as the tool removes material on the sinusoidal surface.

At points 1 and 3 in Fig. 2, the clearance angle is equal to the nominal value so there is no effect due to cutting on the sinusoidal path. However, at point 2 the clearance angle is small (or negative) and the thrust force in the surface normal direction is increased. At point 4, on the other hand, the clearance angle is larger than the nominal and the thrust force is decreased. Because the change in force caused by the sinusoidal path is 90 deg out of phase with the displacement and has the opposite sign from velocity it is considered to be a viscous damping force (i.e., a force that is proportional to velocity).Given the preceding description, the process damping force, F_d, in the y direction can be expressed as a function of velocity, chip width, cutting speed, and a constant C [21]. See Eq. 2.

$$F_d = -C\frac{b}{V}\dot{y} \tag{2}$$

As a final note regarding the sinusoidal path description in Fig. 2, the damping effect is larger for shorter vibration wavelengths, λ, because the slope of the sinusoidal surface increases and, subsequently, the variation in clearance angle increases. The wavelength equation, provided in Eq. 3, shows that lower cutting speeds or higher vibrating frequencies, f, gives shorter wavelengths and, subsequently, increased process damping. This process damping wavelength concept will

be revisited to develop a λ value that is analogous to the C value from Eq. 2.

$$\lambda=\frac{V}{f} \tag{3}$$

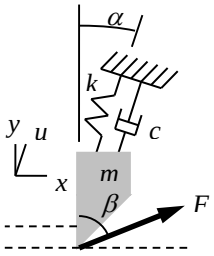

Figure 3. Single degree of freedom turning model.

STABILITY ALGORITHM

Single Degree of Freedom Turning

To describe the stability algorithm, consider the single degree of freedom turning model displayed in Fig. 3. Tlusty [24] defines the limiting stable chip width, $b_{\lim}$, for regenerative chatter using:

$$b_{\lim}=\frac{-1}{2K_S\,\mathrm{Re}(G_{or})}, \tag{4}$$

where G_{or} is the oriented frequency response function, $G_{or}=\cos(\beta-\alpha)\cos(\alpha)G_u$. In this expression, β is the force angle relative to the surface normal, α is the angle between the u direction and the surface normal, and G_u is the frequency response function in the u direction. To relate the frequency-dependent $b_{\lim}$ vector to spindle speed, Ω, Eq. 5 is applied to define the relationship between Ω and the valid chatter frequencies, f_c (i.e., those frequencies where the real part of G_{or} is negative):

$$\frac{f_c}{\Omega}=N+\frac{\varepsilon}{2\pi}, \tag{5}$$

where $N=0,1,2,...$ is the integer number of waves per revolution (i.e., the lobe number) and $\varepsilon=2\pi-2\tan^{-1}\left(\frac{\mathrm{Re}(G_{or})}{\mathrm{Im}(G_{or})}\right)$ (rad) is the phase between the current vibration and the previous pass.

To incorporate the process damping force (which acts in the y direction), it is first projected into the u direction:

$$F_u=F_d\cos(\alpha)=-C\frac{b}{V}\dot{y}\cos(\alpha)=-\left(C\frac{b}{V}\cos(\alpha)\right)\dot{y}. \tag{6}$$

The final form of Eq. 6 emphasizes that the u projection of the process damping force is effectively a viscous damping term. Therefore, the force can be incorporated in the traditional regenerative chatter stability analysis by modifying the structural damping in G_u. As shown in Fig. 3, the single degree of freedom, lumped parameter dynamic model can be described using the mass, m, viscous damping coefficient, c, and spring stiffness, k. In the absence of process damping, the equation of motion in the u direction is:

$$m\ddot{u}+c\dot{u}+ku=F\cos(\beta-\alpha). \tag{7}$$

The corresponding frequency response function in the u direction is:

$$G_u=\frac{U}{F\cos(\beta-\alpha)}=\frac{1}{-m\omega^2+ic\omega+k}, \tag{8}$$

where ω is the excitation frequency (rad/s). When process damping is included, however, the equation of motion becomes:

$$m\ddot{u}+c\dot{u}+ku=F\cos(\beta-\alpha)-\left(C\frac{b}{V}\cos(\alpha)\right)\dot{y}. \tag{9}$$

Replacing $\dot{y}$ in Eq. 9 with $\cos(\alpha)\dot{u}$ gives:

$$m\ddot{u}+c\dot{u}+ku=F\cos(\beta-\alpha)-\left(C\frac{b}{V}\cos^2(\alpha)\right)\dot{u}. \tag{10}$$

Rewriting Eq. 10 to combine the velocity terms yields:

$$m\ddot{u}+\left(c+C\frac{b}{V}\cos^2(\alpha)\right)\dot{u}+ku=F\cos(\beta-\alpha), \tag{11}$$

where the new viscous damping coefficient is $c_{new}=c+C\frac{b}{V}\cos^2(\alpha)$. Replacing the original damping coefficient, c, (from the structure dynamics only) with c_{new} enables process damping to be incorporated in the analytical stability model. The new frequency response function is:

$$G_u=\frac{U}{F\cos(\beta-\alpha)}=\frac{1}{-m\omega^2+ic_{new}\omega+k}. \tag{12}$$

However, the new damping value is a function of both the spindle speed-dependent limiting chip width and

the cutting speed. The cutting speed (m/s) depends on the spindle speed (rpm) and workpiece diameter (m) according to $V=\frac{\pi d}{60}\Omega$. Therefore, the b and Ω vectors must be known in order to implement the new damping value. This leads to the converging nature of the stability analysis that incorporates process damping. The following steps are completed for each lobe number, or N value (see Eq. 5):

1. the analytical stability boundary is calculated with no process damping to identify initial b and Ω vectors
2. these vectors are used to determine the corresponding c_{new} vector
3. the stability analysis is repeated with the new damping value to determine updated b and Ω vectors
4. the process is repeated until the stability boundary converges to its final value.

Milling

Tlusty modified the previously described turning analysis to accommodate the milling process [3]. A primary obstacle to defining an analytical solution for milling stability (aside from the inherent time delay) is the time dependence of the cutting force direction. Tlusty solved this problem by assuming an average angle of the tooth in the cut, ϕ_{ave}, and, therefore, an average force direction. This produced an autonomous, or time invariant, system. He then made use of directional orientation factors, μ_x and μ_y, to first project this force into the x and y mode directions and, second, project these results onto the surface normal (in the direction of ϕ_{ave}). The new $b_{\lim}$ and Ω expressions for milling are provided in Eqs. 13 and 14, where N_t is the number of teeth on the cutter and N_t^* is the average number of teeth in the cut; see Eq. 15, where ϕ_s and ϕ_e (deg) are the start and exit angles defined by the radial depth of cut. The ε equation remains the same as before.

$$b_{\lim}=\frac{-1}{2K_S\,\mathrm{Re}[G_{or}]N_t^*} \tag{13}$$

$$\frac{f_c}{\Omega N_t}=N+\frac{\varepsilon}{2\pi} \tag{14}$$

$$N_t^*=\frac{\varphi_e-\varphi_s}{\frac{360}{N_t}} \tag{15}$$

Up Milling. The process damping force model defined in Eq. 2 was again applied, but the surface normal direction now depends on ϕ_{ave}. The geometry is shown in Fig. 8a, where n is the surface normal direction. The projection of the process damping force from the n direction onto the x direction is:

$$F_x = F_d\cos\left(90-\phi_{ave}\right) = -\left(C\frac{b}{V}\cos(90-\phi_{ave})\right)\dot{n}\,. \tag{16}$$

Note that the velocity term is now $\dot{n}$. Substituting $\dot{n}=\cos(90-\phi_{ave})\dot{x}$ in Eq. 16 gives:

$$F_x=-\left(C\frac{b}{V}\cos^2(90-\phi_{ave})\right)\dot{x}\,. \tag{17}$$

The new damping in the converging stability calculation for the x direction frequency response function, G_x, is therefore:

$$c_{new,x}=c_x+C\frac{b}{V}\cos^2(90-\phi_{ave})\,. \tag{18}$$

The new y direction damping is:

$$c_{new,y}=c_y+C\frac{b}{V}\cos^2(180-\phi_{ave})\,. \tag{19}$$

The oriented frequency response function for this case is $G_{or}=\mu_x G_x+\mu_y G_y$, where $\mu_x=\cos(\beta-(90-\phi_{ave}))\cos(90-\phi_{ave})$ and $\mu_y=\cos(180-\phi_{ave}-\beta)\cos(180-\phi_{ave})$.

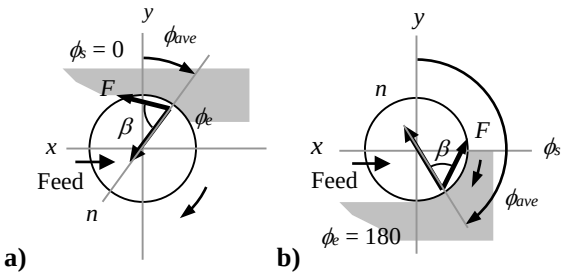

Figure 8. a) Geometry for up milling using the average tooth angle stability analysis (a 25% radial immersion cut is shown for illustrative purposes). b) Model for down milling (a 50% radial immersion cut is shown). The vector n defines the average surface normal direction.

Down Milling. The geometry for the down milling case is shown in Fig. 8b. Using the same approach as described in the up milling case, the x and y direction damping values are provided in Eqs. 20 and 21.

$$c_{new,x}=c_x+C\frac{b}{V}\cos^2(\phi_{ave}-90) \quad (20)$$

$$c_{new,y}=c_y+C\frac{b}{V}\cos^2(180-\phi_{ave}) \quad (21)$$

The oriented frequency response function for this case is $G_{or}=\mu_x G_x+\mu_y G_y$, where $\mu_x=\cos(\beta+\phi_{ave}-90)\cos(\phi_{ave}-90)$, and $\mu_y=\cos(\beta-(180-\phi_{ave}))\cos(180-\phi_{ave})$.

EXPERIMENT DESCRIPTIONS

The process damping coefficient, specific cutting force coefficients, and tool life model coefficients for selected tool-workpiece pairs were identified through a series of cutting tests. Single-tooth indexable end mills were used to mill AISI 1018 steel, 6Al-4V titanium, and 304 stainless steel workpieces secured to the top of single degree-of-freedom leaf-type flexure.

Setup Description

To enable convenient control of the system dynamics, a single degree-of-freedom, parallelogram leaf-type flexure was constructed to provide a flexible foundation for individual workpieces; see Fig 9. Because the flexure compliance was much higher than the tool-holder-spindle-machine, the stability analysis was completed using only the flexure's dynamic properties. The modal parameters for the flexure are provided in Table 1. The *x* and *y* directions correspond to the flexible and stiff directions of the flexure, respectively, where *x* is the feed direction.

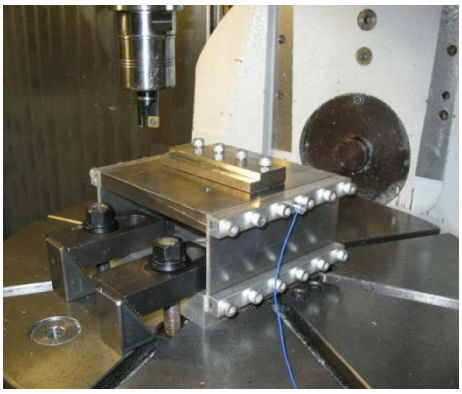

Figure 9. Setup for milling stability tests. An accelerometer was used to measure the vibration signal during cutting.

An accelerometer (PCB Piezotronics model 352B10) was used to measure the vibration during cutting. The frequency content of the accelerometer signal was used in combination with the machined surface finish to establish stable/unstable performance, i.e., cuts that exhibited significant frequency content at the flexure's *x* direction natural frequency, rather than the tooth passing frequency, were considered to be unstable.

Table 1. Modal parameters for the flexure setup.

Direction	Viscous damping ratio	Modal stiffness ($\times 10^6$ N/m)	Natural frequency (Hz)
x	0.063	2.77	228
y	0.037	174	1482

In order to study the influence of relief angle, two single-tooth indexable square end mills of similar diameter were used: 1) 18.54 mm diameter with a 15 deg relief angle (Kennametal model KICR-0.73-SD3-033.3C); and 2) 19.05 mm diameter with an 11 deg relief angle (Cutting Tool Technologies model DRM-03). Both cutting tools had zero deg rake and helix angles and the TiN-coated inserts had no edge preparation.

Process Damping Coefficient Identification

A grid of test points at low spindle speed was selected to investigate the process damping behavior for each tool-material combination. Based on the stable/unstable cutting test results, a single variable residual sum of squares (*RSS*) estimation was applied to identify the process damping coefficient, *C*, that best represented the experimental stability boundary [22-23].

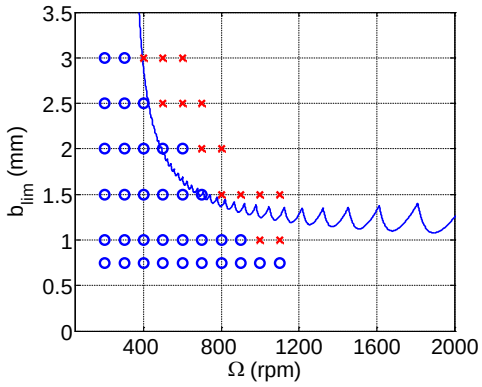

Figure 10. Stability boundary for 50% radial immersion, 15 deg relief angle, low wear up milling tests in 1018 steel ($C = 1.3\times10^5$ N/m).

Using the minimum *RSS* method, stability testing was performed for both endmills. Because flank wear can

affect the process damping behavior, the flank wear width (FWW) was limited to less than 100 μm for a first set of tests (low wear) and was maintained between 150 μm and 250 μm for a second set (moderate wear). The stability boundary and 1018 steel test cut results for the 18.54 mm diameter, 15 deg relief angle endmill under low wear conditions are presented in Fig. 10 as an example.

Specific Cutting Force Coefficient Measurement

The specific cutting force coefficients were identified under stable cutting conditions using a cutting force dynamometer (Kistler model 9257B). A linear regression to the mean cutting force from a series of tests at incremented feed per tooth values was used to identify the cutting force model values [25]. Because process damping is recognized to be sensitive to flank wear, the coefficients were measured at a flank wear width (FWW) less than 100 μm for low wear conditions and between 150 μm and 250 μm for moderate wear conditions.

Tool Wear Effects

In order to explore the effect of tool wear on the process damping performance, tests were completed using worn tools where the FWW was maintained between 150 μm and 250 μm at a nominal level of 200 μm. For the 15 deg relief angle tool in 1018 steel, for example, the process damping coefficient increased by 20% (1.3×10^5 N/m to 1.5×10^5 N/m) from the low to moderate wear conditions. Because the tool naturally wears, particularly for the hard-to-machine materials considered in this study, a Taylor tool life model was established for each tool-material combination. Although more recent tool life models have been presented, Taylor's model was selected due to its widespread familiarity. The reason for obtaining tool life parameters was to establish an appropriate cutting speed range and avoid prohibitive tool wear for the selected tool-material combinations.

Tool life, *T*, is generally defined as the time required to obtain a predetermined wear level. Depending on the dominant wear mode, the wear level may be described using the flank wear width (FWW), crater depth, and/or notch depth. The Taylor tool life equation relates the tool life to the cutting speed using a power law model [26]:

$$VT^{n_T} = C_T . \tag{22}$$

where n_T and C_T are empirical constants. Wear tests were completed using the 18.54 mm diameter single-tooth indexable square endmill (15 deg relief angle). The chip load was 0.05 mm/tooth for the 25% radial immersion down milling cuts and a water miscible mist coolant with a flow rate of approximately 15-20 ml/min was applied. The primary mode of tool wear in all cases was flank wear; see Fig. 11. To avoid removing the inserted tool from the spindle, a portable digital microscope was used to record the FWW at regular intervals as shown in Fig. 12. The tool life was defined as the time required to reach a maximum FWW of 0.3 mm. There was an uncertainty in each FWW measurement due to the repeatability of the angular orientation of the microscope relative to the cutting edge. This variation proved to be negligible, but care was taken to ensure the cutting edge was approximately in the same angular orientation for each measurement. Tests were completed at cutting speeds of V = {29.1, 58.2, and 174.7} m/min, which correspond to spindle speeds of Ω = {500, 1000, and 3000} rpm. The values for n_T and C_T were identified using a least squares curve fit to the (V, T) data points.

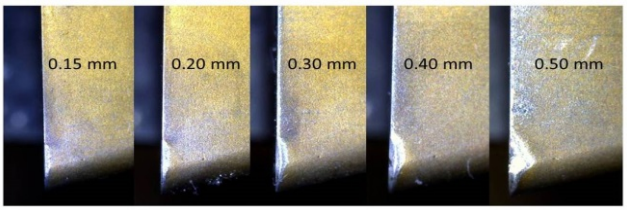

Figure 11. Sample measurements of the maximum FWW progression during wear tests.

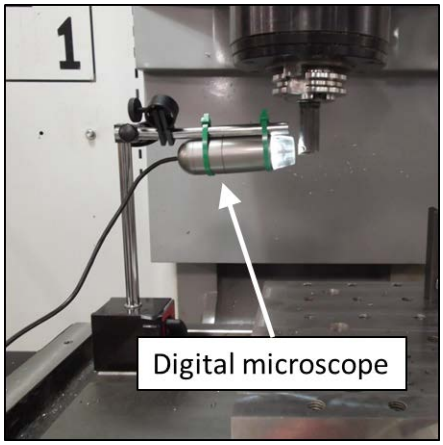

Figure 12. Setup for interrupted FWW measurements.

Figure 13 displays the FWW progression versus cutting time for 6Al-4V titanium. The 'o' symbols represent the intervals at which the FWW was recorded. As expected, the wear rate was found to increase as cutting speed was increased. The tool life (min) was then plotted versus the cutting speed (m/s) and a power law curve was fit to the data. Figure 14 displays the curve fit through the three data points for 6Al-4V titanium (R^2 = 0.97). It is observed that cutting operations are limited to

spindle speeds less than 1000 rpm if a tool life greater than approximately 30 min is desired. As a practical limit, this range of spindle speeds was used to select the operating speed range for process damping characterization.

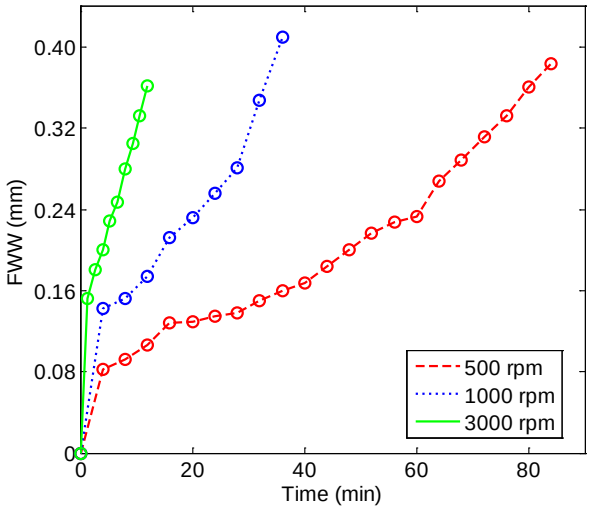

Figure 13. Increase in FWW with cutting time at three spindle speeds for 6Al-4V titanium.

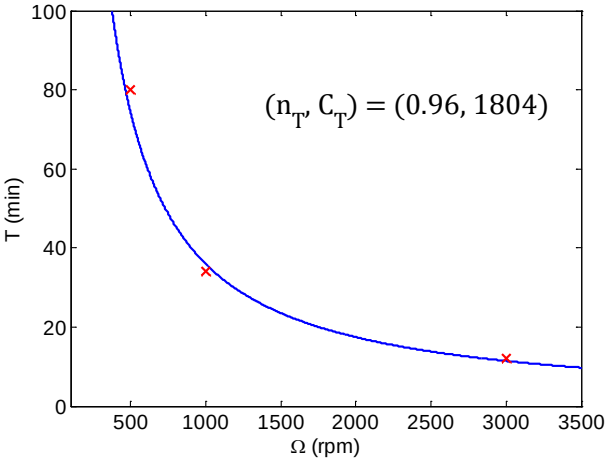

Figure 14. Taylor tool life model fit for 6Al-4V titanium.

DATABASE

The database of process modeling coefficients for 1018 steel, 6Al-4V titanium, and 304 stainless steel is presented in this section. The database includes coefficients for the process damping model, specific cutting force, and Taylor tool life model. Additionally, a wavelength parameter is presented that enables the traditional analytical stability model to be augmented to incorporate the process damping stability increase observed at low cutting speeds.

As described previously, process damping can be described as an interference phenomenon between the relief face of the tool and the machined surface. As the wavelength of the surface undulations decreases for a fixed amplitude, the likelihood of energy dissipation through this interference increases. Therefore, process damping can be modeled as a function of the wavelength, where a shorter wavelength gives increased stability. In this study, the functional form:

$$\Lambda = b_{cr} e^{\frac{1}{(\Omega\lambda)^2}}. \tag{23}$$

was selected, where Λ defines the process damping behavior, b_{cr} is the critical (asymptotic) stability limit from the traditional stability analysis, Ω is expressed in rpm, and λ is the wavelength parameter (in m). Note that Λ takes the units of b_{cr}. Figure 15 shows the process damping stability limit and Λ for 50% radial immersion, 15 deg relief angle, low wear up milling tests in 1018 steel (C = 1.3×10^5 N/m, λ = 2.2×10^{-3} m). For the traditional stability analysis that does not include process damping, Λ could be superimposed on the stability limit to identify the new, low cutting speed stability boundary. Each λ was selected based on the minimum residual sum of squares (RSS) between the b_{cr} curve that includes process damping and Λ.

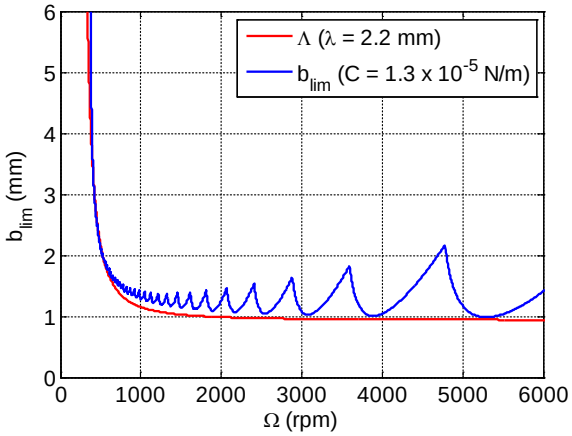

Figure 15. Stability boundary for 50% radial immersion, 15 deg relief angle, low wear up milling tests in 1018 steel (C = 1.3×10^5 N/m) with multiplier, M (λ = 2.2×10^{-3} m).

The process damping coefficients (C and λ) are presented in Table 2, the cutting force coefficients (K_s and β) in Table 3, and the tool life model parameters (n_T and C_T) in Table 4. Note that both low wear and moderate

wear values are presented for the process damping and cutting force coefficients. In Tables 2 and 3, the cutting conditions for 1018 steel were 50% radial immersion up milling. They were 25% radial immersion down milling for the other two materials. This increased the allowable axial depths of cut and eliminated chip welding to the machined surface.

Table 2. Process damping coefficients.

Low insert wear (FWW < 100 μm)				
	11 deg relief angle (19.05 mm diameter)		15 deg relief angle (18.54 mm diameter)	
Material	C ($\times 10^5$ N/m)	λ (mm)	C ($\times 10^5$ N/m)	λ (mm)
1018 steel	1.6	1.8	1.3	2.2
6Al-4V titanium	1.7	1.0	1.2	1.5
304 stainless steel	5.2	0.47	4.1	0.62
Moderate insert wear (150 μm < FWW < 250 μm)				
1018 steel	2.0	1.5	1.5	1.9
6Al-4V titanium	1.8	0.86	1.4	1.0
304 stainless steel	5.8	0.44	4.5	0.55

*The cutting conditions for 1018 steel were 50% radial immersion up milling. They were 25% radial immersion down milling for the other two materials.

Table 3. Specific cutting force coefficients.

Low insert wear (FWW < 100 μm)				
	11 deg relief angle (19.05 mm diameter)		15 deg relief angle (18.54 mm diameter)	
Material	K_s (N/mm^2)	β (deg)	K_s (N/mm^2)	β (deg)
1018 steel	2531.0	62.0	2359.1	63.5
6Al-4V titanium	2107.0	66.0	2076.3	66.7
304 stainless steel	3318.0	62.5	3427.2	63.1
Moderate insert wear (150 μm < FWW < 250 μm)				
1018 steel	2550.2	62.0	2441.0	63.5
6Al-4V titanium	2131.2	60.1	2247.2	56.3
304 stainless steel	3517.0	61.0	3503.2	61.5

Table 4. Taylor tool life model parameters.

Material	n_T	C_T	R^2
1018 steel*	0.34	649	0.95
6Al-4V titanium	0.96	1804	0.97
304 stainless steel	0.67	1484	0.98

*Values were obtained from testing performed by Karandikar *et al.* [27] using the same tool geometry, but an uncoated insert and 50% radial immersion up milling.

From Table 2, it is seen that the process damping force coefficient, C, increases with progressive wear and decreases with a larger relief angle; a larger C value indicates more process damping. Both trends support the general description of process damping as interference between the relief face and machined surface. Increased flank wear reduces the apparent relief angle local to the cutting edge. A smaller relief angle, whether by design or via wear, encourages the interference phenomenon. The converse relationship is observed for λ. A larger value of λ indicates reduced process damping, so smaller values of λ are obtained for increased wear and smaller relief angles.

For the specific cutting force coefficient, K_s, no clear trend is apparent for a change in the wear state or tool geometry. The largest difference for relief angle variation is 6.8% (1018 steel). The largest difference due to the wear level is -8.2% (15 deg relief angle tool, 6Al-4V titanium).

CONCLUSIONS

An analytical solution for milling stability that incorporates process damping was provided, where the process damping force model was based on a single coefficient, C. This is analogous to the specific cutting force approach to modeling force magnitude. A database was established to tabulate not only the process damping coefficient, but also the cutting force model coefficients, and Taylor tool life model parameters. Additionally, a wavelength value, λ, was presented to predict the low cutting speed increase in the allowable depth of cut using an exponential function. Process damping and cutting

force parameters were reported for both low and moderate wear levels.

Stability testing was completed using a parallelogram, leaf-type flexure to identify the process damping behavior for low-speed milling. The workpiece materials were AISI 1018 steel, 6Al-4V titanium, and 304 stainless steel. Two inserted cutting tools were used with relief angles of 11 deg and 15 deg; the rake and helix angles were zero for both single-insert cutters. It was demonstrated that a reduction in the relief angle and an increase in flank wear on the cutting edge resulted in an increased process damping effect. Expected trends of increasing C and decreasing λ with more significant process damping were observed.

Process damping is particularly important for hard-to-machine materials. In these instances, tool wear generally prohibits higher surface speeds and the use of the large stable zones available at the corresponding high spindle speeds. This limits the spindle speed to low values, which decreases the material removal rate. However, by exploiting process damping, higher stable axial depths and material removal rates can be achieved. The goal of this work was to develop a database of model parameters that would enable pre-process selection of machining parameters that provide high productivity.

ACKNOWLEDGEMENTS

The authors gratefully acknowledge partial financial support from the UNC Charlotte Center for Precision Metrology Affiliates Program and the 2013-14 Siemens Energy Graduate Scholarship (for C. Tyler).

REFERENCES

[1] J. Tlusty, M. Polacek, The stability of machine tools against self-excited vibrations in machining, in: Proceedings of the ASME International Research in Production Engineering Conference, Pittsburgh, PA, 1963, pp. 465-474.

[2] S.A. Tobias, Machine Tool Vibrations, Blackie and Sons, Ltd., Glasgow, 1965.

[3] J. Tlusty, W. Zaton, F. Ismail, Stability lobes in milling, Annals of the CIRP, 32/1 (1983) 309-313.

[4] Y. Altintas, E. Budak, Analytical prediction of stability lobes in milling, Annals of the CIRP, 44/1 (1995) 357-362.

[5] P.W. Wallace, C. Andrew, Machining forces: Some effects of tool vibration, Journal of Mechanical Engineering Science, 7 (1965) 152-162.

[6] T.R. Sisson, R.L. Kegg, An explanation of low-speed chatter effects, Journal of Engineering for Industry, 91 (1969) 951-958.

[7] J. Peters, P. Vanherck, H. Van Brussel, The measurement of the dynamic cutting coefficient, Annals of the CIRP, 21/2 (1971) 129-136.

[8] J. Tlusty, Analysis of the state of research in cutting dynamics, Annals of the CIRP, 27/2 (1978) 583-589.

[9] D.W. Wu, A new approach of formulating the transfer function for dynamic cutting processes, Journal of Engineering for Industry, 111 (1989) 37-47.

[10] M.A. Elbestawi, F. Ismail, R. Du, B.C. Ullagaddi, Modelling machining dynamics damping in the tool-workpiece interface, Journal of Engineering for Industry, 116 (1994) 435-439.

[11] B.Y. Lee, Y.S. Trang, S.C. Ma, Modeling of the process damping force in chatter vibration, International Journal of Machine Tools and Manufacture, 35 (1995) 951-962.

[12] F. Abraria, M.A. Elbestawi, A.D. Spencea, On the dynamics of ball end milling: Modeling of cutting forces and stability analysis, International Journal of Machine Tools and Manufacture, 38 (1998) 215-237.

[13] K. Ahmadi, F. Ismail, Machining chatter in flank milling, International Journal of Machine Tools and Manufacture, 50 (2010) 75-85.

[14] C.Y. Huang, J.J. Wang, Mechanistic modeling of process damping in peripheral milling, Journal of Manufacturing Science and Engineering, 129 (2007) 12-20.

[15] Y.S. Chiou, E.S. Chung, S.Y. Liang, Analysis of tool wear effect on chatter stability in turning, International Journal of Mechanical Sciences, 37 (1995) 391-404.

[16] R.Y. Chiou, S.Y. Liang, Chatter stability of a slender cutting tool in turning with tool wear effect, International Journal of Machine Tools and Manufacture, 38 (1998) 315-327.

[17] N.K. Chandiramani, T. Pothala, Dynamics of 2-dof regenerative chatter during turning, Journal of Sound and Vibration, 290 (2006) 448-464.

[18] K. Jemielniak, A. Widota, Numerical simulation of non-linear chatter vibration in turning, International Journal of Machine Tools and Manufacturing, 29 (1989) 239-247.

[19] K. Ahmadi, F. Ismail, Experimental investigation of process damping nonlinearity in machining chatter, International Journal of Machine Tools and Manufacture, 50 (2010) 1006-1014.

[20] E. Budak, L.T. Tunc, A new method for identification and modeling of process damping

in machining, Journal of Manufacturing Science and Engineering, 131 (2009) 051019/1-10.

[21] Y. Altintas, M. Eynian, H. Onozuka, Identification of dynamic cutting force coefficients and chatter stability with process damping, Annals of the CIRP, 57/1 (2008) 371-374.

[22] C. Tyler, T. Schmitz, T., Process damping analytical stability analysis and validation, Transactions of the NAMRI/SME, 40 (2012).

[23] C. Tyler, T. Schmitz, T., Analytical process damping stability prediction, Journal of Manufacturing Processes, 15 (2013) 69-76.

[24] J. Tlusty, Manufacturing Processes and Equipment, Prentice Hall, Upper Saddle River, NJ, 2000.

[25] T. Schmitz, S. Smith, Machining Dynamics: Frequency Response to Improved Productivity, Springer, New York, NY, 2009.

[26] F.W. Taylor, On the art of cutting metals, Transactions of the ASME, (1906) 31-248.

[27] J. Karandikar, A. Abbas, T. Schmitz, Tool life prediction using random walk Bayesian updating, Machining Science and Technology, 17/3 (2013) 410-442.